Theoretical Investigations Toward the Asymmetric Insertion Reaction of Diazoester with Aldehyde Catalyzed by N-Protonated Chiral Oxazaborolidine: Mechanisms and Stereoselectivity.

ARTICLE *in* THE JOURNAL OF PHYSICAL CHEMISTRY A · JULY 2015

Impact Factor: 2.69 · DOI: 10.1021/acs.jpca.5b04793 · Source: PubMed

4 AUTHORS, INCLUDING:

Yang Wang
Zhengzhou University
14 PUBLICATIONS **43** CITATIONS
SEE PROFILE

Mingsheng Tang
Zhengzhou University
95 PUBLICATIONS **1,378** CITATIONS
SEE PROFILE

Donghui Wei
Zhengzhou University
65 PUBLICATIONS **512** CITATIONS
SEE PROFILE

THE JOURNAL OF PHYSICAL CHEMISTRY A

Article

pubs.acs.org/JPCA

Theoretical Investigations toward the Asymmetric Insertion Reaction of Diazoester with Aldehyde Catalyzed by N-Protonated Chiral Oxazaborolidine: Mechanisms and Stereoselectivity

Yang Wang, Xiaokang Guo, Mingsheng Tang,* and Donghui Wei*

The College of Chemistry and Molecular Engineering, Center of Computational Chemistry, Zhengzhou University, Zhengzhou, Henan Province 450001, P. R. China

Supporting Information

ABSTRACT: In recent years, the N-protonated chiral oxazaborolidine has been utilized as the Lewis acid catalyst for the asymmetric insertion reaction, which is one of the most challenging topics in current organic chemistry. Nevertheless, the reaction mechanism, stereoselectivity, and regioselectivity of this novel insertion reaction are still unsettled to date. In this present work, the density functional theory (DFT) investigation has been performed to interrogate the mechanisms and stereoselectivities of the formal C−C/H insertion reaction between benzaldehyde and methyl α-benzyl diazoester catalyzed by the N-protonated chiral oxazaborolidine. For the reaction channel to produce the *R*-configured C−C insertion product as the predominant isomer, the catalytic cycle can be characterized by four steps: (i) the complexation of the aldehyde with catalyst, (ii) addition of the other reactant methyl α-benzyl diazoester, (iii) the removal of nitrogen concerted with the migration of phenyl group or hydrogen, and (iv) the dissociation of catalyst from the products. Our computational results show that the carbon−carbon bond formation step is the stereoselectivity determining step, and the reaction pathways associated with [1, 2]-phenyl group migration occur preferentially to those pathways associated with [1, 2]-hydrogen migration. The pathway leading to the *R*-configured product is the most favorable pathway among the possible stereoselective pathways. All these calculated outcomes align well with the experimental observations. The novel mechanistic insights should be valuable for understanding this kind of reaction.

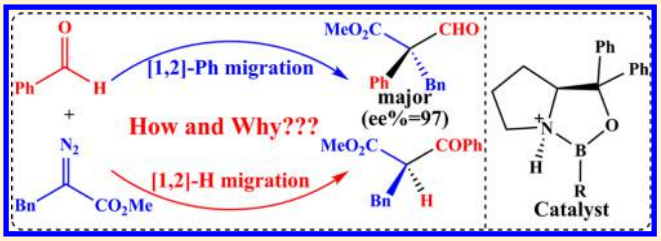

1. INTRODUCTION

Chiral boron salts possess proper Lewis acidities and electrophilic activities, and have been successfully utilized in many organic reactions as chiral Lewis acid catalysts over the past decades.[1−9] The most famous example is the CBS (Corey−Bakshi−Shibate) chiral oxazaborolidine catalyst,[10,11] which has been found to be an important variety of compounds working as the Lewis acid catalysts for the enantio- and diastereoselective reduction of highly functionalized ketones in the presence of BH_3. In the general mechanistic model, the Lewis basic nitrogen atom of the oxazaborolidine serves to activate BH_3 as a hydrogen donor by the coordination with the electrophilic BH_3, which also increases strongly the Lewis acidity of the endocyclic boron atom. As in the CBS reduction, the Lewis acidic boron center in oxazaborolidine is assumed to be activated by the attachment of proton or Lewis acid to the adjacent nitrogen atom in the catalytic reactions. The CBS catalyst offers excellent results with a wide variety of polyfunctional ketones, making this methodology very useful in several fields of organic synthesis, like those of natural organic substances, chiral building blocks, and bioactive compounds. Application of the oxazaborolidine-catalyzed asymmetric reduction was eventually extended to oxime and imines to afford chiral amines or hydroxylamines.[12−15]

Recent publications indicated that the protonated or Lewis acid promoted oxazaborolidines also performed well as powerful organocatalysts in the Diels−Alder reactions. Corey and co-workers developed the enantioselective Diels−Alder reactions catalyzed by Brønsted acid (TfOH of Tf_2NH) and Lewis acid ($AlBr_3$ or BBr_3) promoted oxazaborolidine.[16−19] Yamamoto et al. reported the first example of enantio- and regioselective Diels−Alder reaction of both 1- and 2-substituted cyclopentadienes mediated by a Brønsted acid activated chiral oxazaborolidine.[20] Subsequently, they demonstrated the Lewis acid activated chiral oxazaborolidine catalyzed the enantioselective Diels−Alder reactions for stereoselective construction of halogenated quaternary centers.[21] In addition, the Diels−Alder reaction catalyzed by the activated oxazaborolidine was also studied theoretically. Sherhurn et al. first reported the computational investigations into a Brønsted acid activated chiral oxazaborolidine catalyzed asymmetric Diels−Alder reaction.[22] They validated Corey's pre-transition-state models with aldehyde- and ester-activated dienophiles, and further indicated an alternative coordination mode for esters without a C−H···O hydrogen bond. Fujimoto and co-workers' theoretical

Received: May 19, 2015
Revised: July 1, 2015
Published: July 8, 2015

DOI: 10.1021/acs.jpca.5b04793
J. Phys. Chem. A 2015, 119, 8422−8431

study demonstrated that the coordination of the Lewis acid $AlBr_3$ to the nitrogen atom of oxazaborolidine enhances the Lewis acidity of its boron center and enables it to coordinate to methacrolein in the Diels–Alder reaction between cyclopentadiene and methacrolein.[23] Zain's group computationally investigated the mechanism and enantioselectivity of the organocatalytic and uncatalyzed Diels–Alder reaction, and also validated the Corey's predictive selection rules.[24] Houk and co-workers investigated the Corey's cationic oxazaborolidine-catalyzed Diels–Alder reactions using DFT calculations and predicted the experimental enantioselectivity exactly.[25] Furthermore, chemists also found that this kind of oxazaborolidinium salt can be an efficient catalyst in many other asymmetric syntheses, such as cycloaddition reactions (i.e., [2 + 2] cycloaddition reaction,[26] [3 + 2] cycloaddition,[27] and 1,3-dipolar cycloaddition[28]), bicyclization reactions,[29] cyanosilylation of aldehydes/ketones,[30,31] Micheal additions,[32] Mukaiyama-Aldol reaction,[33,34] and so on.[35−37]

However, the N-protonated chiral oxazaborolidine utilized as the catalyst for the asymmetric formal insertion of diazoester into the aryl-CHO bond, which is one of the most challenging topics in current organic chemistry, has been rarely reported in experiment. Recently, Ryu and co-workers reported the C–H insertion reactions catalyzed by N-protonated chiral oxazaborolidine,[38−40] which reveal that the N-protonated chiral oxazaborolidine is a suitable catalyst for this kind of asymmetric insertion reaction. More recently, they reported the first example of the catalytic enantioselective route to synthesize functionalized all-carbon quaternary acyclic systems via the stereoselective formal C–C/H insertion of diazoesters into aryl-CHO bond catalyzed by the N-protonated chiral oxazaborolidine,[41] which can allow the [1, 2]-migration of an aryl group in preference to a hydrogen (Scheme 1). To the best of our knowledge, the theoretical study on the mechanisms of the C–C/H insertion reactions catalyzed by the N-protonated chiral oxazaborolidine catalyst has not been reported by now.

Scheme 1. N-Protonated Chiral Oxazaborolidine Catalyzed C–C/H Insertion Reaction

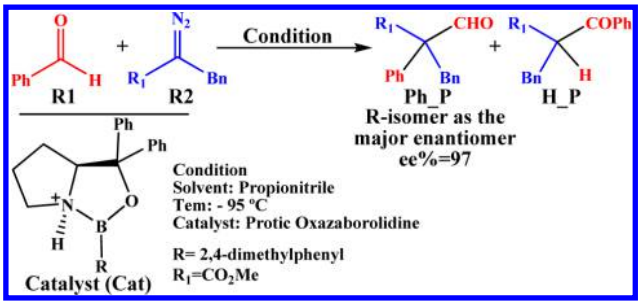

Herein, we attempt in this study to disclose the electronic mechanism of the N-protonated oxazaborolidine in this novel insertion reaction of aldehyde with diazoester (Scheme 1) reported by Ryu and co-workers. Moreover, there are still some questions which need to be answered for the novel organocatalytic reaction: (1) How does this kind of reaction happen in detail? (2) Which is the stereoselectivity determining step? (3) What are the factors that control the stereoselectivities of the title reaction? (4) How can the N-protonated oxazaborolidine catalyze the C–C/H insertion reactions? All of the above questions promote us to not only theoretically investigate the competing catalytic reaction mechanisms and regio- and enantioselectivity, but also explore the factors that control the stereochemistry of this reaction and the role of the organocatalyst in this kind of reaction.

For the sake of convenience, we denote the N-protonated chiral oxazaborolidine catalyst as **Cat** (Scheme 1), and the benzaldehyde and methyl α-benzyl diazoester (Scheme 1) as **R1** and **R2**, respectively. In this present study, we perform the computational study for the possible reaction mechanisms using density functional theory (DFT), which has been widely utilized in the study of organic,[42−50] biological reaction mechanisms,[51−55] and other aspects.[56−61]

2. COMPUTATIONAL DETAILS

The geometrical optimizations of the reactants, transition states, intermediates, and products in all the possible reaction pathways were carried out using the gradient-corrected function of Becke and of Lee, Yang, and Parr (B3LYP)[62−64] for exchange and correction, with the standard 6-31G(d, p) basis set as implemented in Gaussian 09.[65] The selected functional method has been confirmed to be proper for the CBS catalytic system[66−70] and other theoretical investigations.[71−75] Solvation by propionitrile was taken into account for all calculations (optimizations and frequencies) by a relatively simple self-consistent reaction field (SCRF) method, which is based on the integral equation formalism polarizable continuum model (IEF-PCM).[76,77] In the procedure, the solvent is assimilated as a continuous medium, characterized by the dielectric constant (ε = 27.7), which surrounds a molecule-shape cavity in which the solute is placed. Most significant structures had been represented in the figures by using CYLView.[78]

The stationary points were characterized by frequency calculations in order to verify that each structure was a minimum or a transition state. The same level of intrinsic reaction coordinate (IRC)[79,80] calculations was also carried out to verify that the transition state connects correctly to expect local minima, and the natural bond orbital (NBO)[81−83] analysis was employed to assign the atomic charges. The energies discussed in this paper are based on the electronic energy corrected for the zero-point vibrational energies (ZPVEs).

3. RESULTS AND DISCUSSION

It is a crucial but usually challenging issue to figure out how the catalyst will first exert its effect on reactants for a catalytic reaction. The answers might be different due to the various factors such as the specific structure of the catalyst, the reactant counterparts, and experimental conditions, which are important for the catalytic reactions. In the general view of the reaction catalyzed by Lewis acid oxazaborolidine, the electron-deficient boron atom coordinates with the electron-rich carbonyl oxygen atom. On the basis of this point, the possible reaction mechanisms for this kind of reaction have been suggested and studied, and the detailed discussion has been presented as follows.

3.1. Mechanism Proposal. As shown in Scheme 2, we have investigated the fundamental catalytic cycle for the title reaction, in which the catalyst (**Cat**) exerts its effect on the aldehyde (**R1**).

There are two competing regioselective cycles: (i) the formal C–H bond insertion reaction of aldehyde by alkyldiazoester via the [1, 2]-hydrogen migration (left side of Scheme 2), and (ii) the formal C–C bond insertion of alkyldiazoester into aryl-CHO via the [1, 2]-phenyl group migration (right side of

DOI: 10.1021/acs.jpca.5b04793
J. Phys. Chem. A 2015, 119, 8422−8431

Scheme 2. Possible Competing Pathways for the C−C/H Insertion Reaction

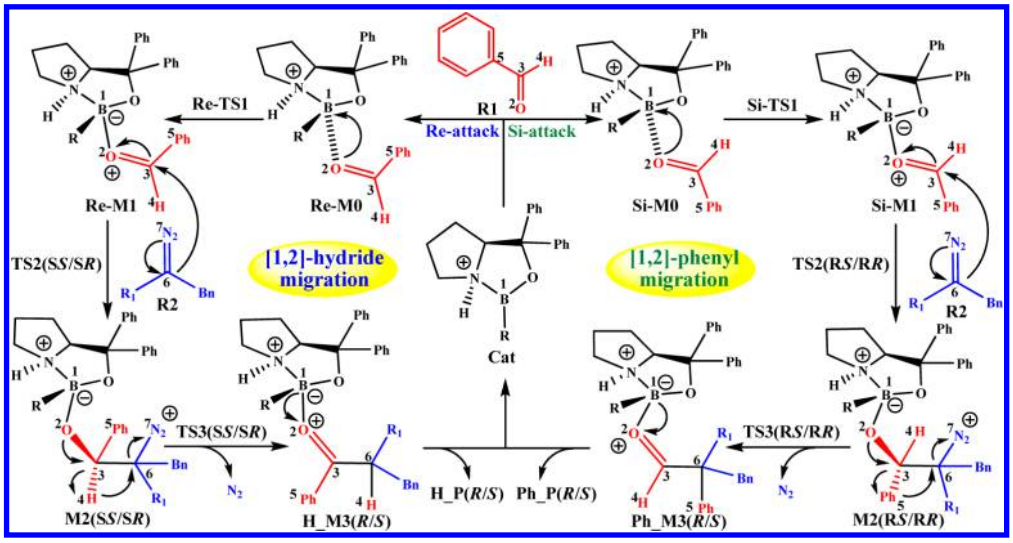

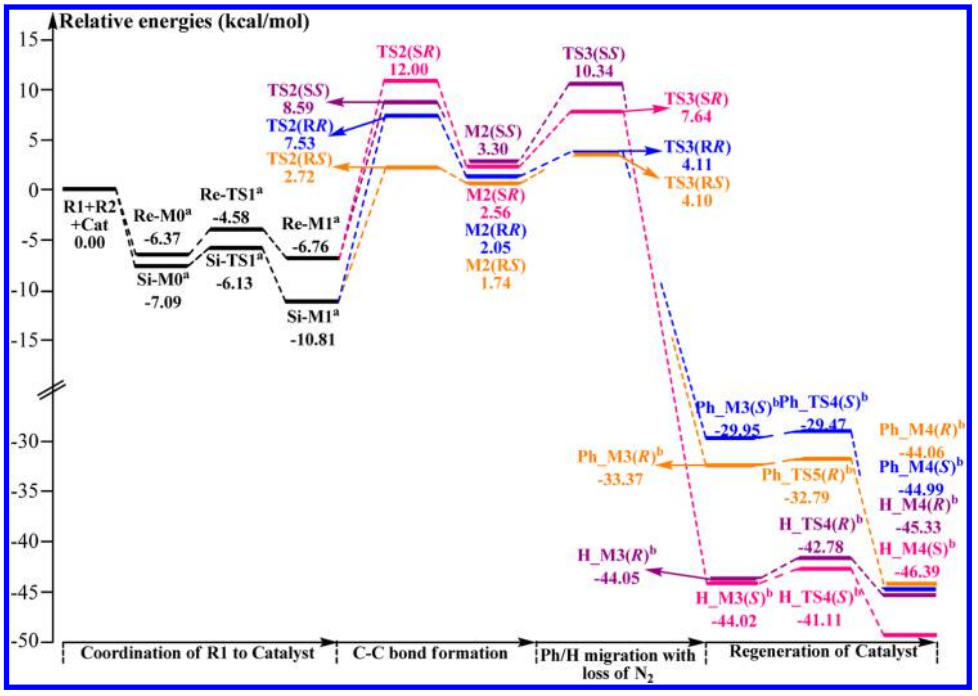

Figure 1. Energy profiles of the chiral protonated oxazaborolidine catalyst catalyzed the formal C−C/H insertion reaction: a indicates adding the energy of R2; b indicates adding the energy of N_2.

Scheme 2). There are generally four steps in both of the two competing catalytic cycles, including (1) the electrophilic attack on benzaldehyde **R1** by catalyst **Cat** to form the coordination intermediate **Re/Si-M1** via transition state **Re/Si-TS1**; (2) the C−C bond formation reaction between intermediate **Re/Si-M1** and **R2** to afford the intermediate **M2(RR/RS/SR/SS)** via transition state **TS2(RR/RS/SR/SS)**; (3) the release of N_2 concerted with the regioselective migration of hydrogen or phenyl group to form the zwitterionic intermediates **M3** (**H_M3(*R*/*S*)** and **Ph_M3(*R*/*S*)**) via transition states **TS3(SS/SR/)** (associated with **H_M3(*R*/*S*)**) and **TS3(RS/RR)** (associated with **Ph_M3(*R*/*S*)**), respectively, and (4) the regeneration of catalyst **Cat**. It should be noted that the prefix "**H_**" represents the formal C−H insertion reaction of aldehyde via [1, 2]-hydrogen migration, while the prefix "**Ph_**" represents the formal C−C insertion reaction of diazoester into aryl-CHO via [1, 2]-migration of phenyl group. We also marked the chirality of the C3 atom in bold **R/S** and the chirality of C6 atom in bold and italic ***R*/*S*** for the sake of clarity. Figure 1 presents the energy profiles of the entire fundamental pathways. The detailed mechanistic discussions have been provided step by step.

3.1.1. ***First Step:*** *Complexation of* ***R1*** *with Catalyst* ***Cat.*** The first step is the formation of a Lewis acid−base complex between the N-protonated chiral oxazaborolidine (**Cat**) and the benzaldehyde (**R1**). The different complexation patterns between the different prochiral faces of catalyst and reactant complexes pose a considerable challenge from the computational point of view.[84] Initially, the reaction precursors **Re/Si-M0** are formed by weak interactions between **R1** and **Cat**, and then the coordinated intermediates **Re/Si-M1** are formed

DOI: 10.1021/acs.jpca.5b04793
J. Phys. Chem. A 2015, 119, 8422−8431

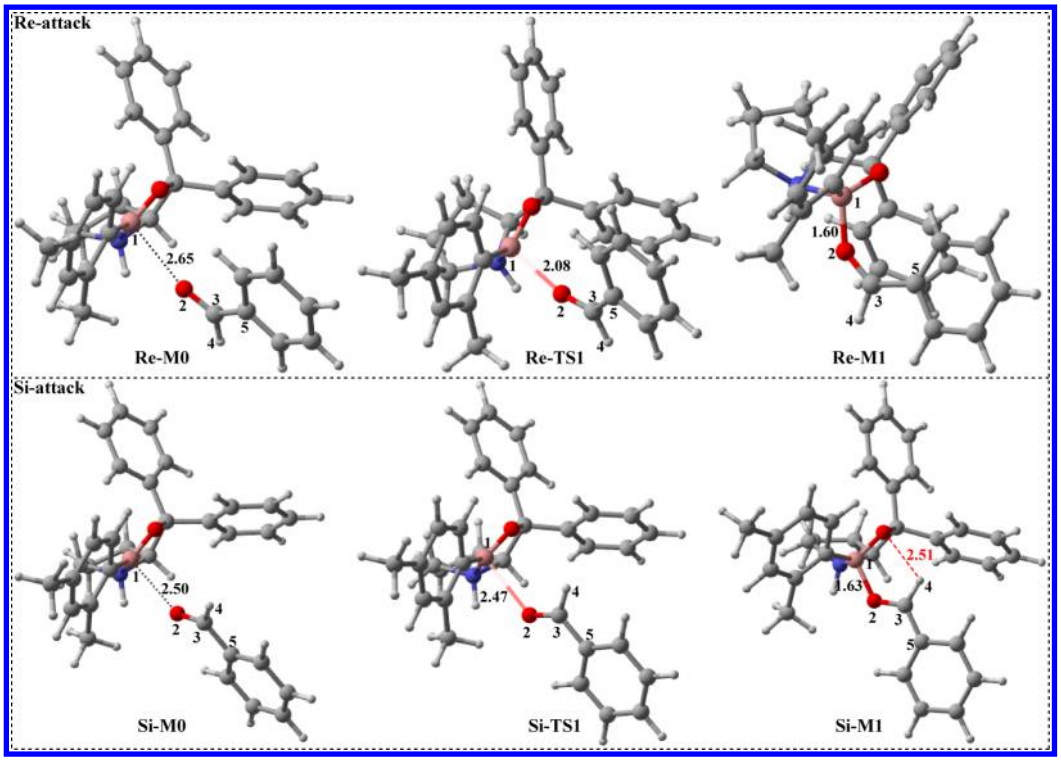

Figure 2. Optimized structures involved in the first step (distances in Å).

through the electrophilic attacks on the O2 atom of **R1** by the B1 atom in **Cat** via transition states **Re/Si-TS1**, respectively.

Figure 2 presents the optimized structures and geometrical parameters involved in the first step. The distance between B1 and O2 atoms is shortened from 2.65/2.50 Å in **Re/Si-M0** to 2.08/2.47 Å in **Re/Si-TS1**, and finally to 1.60/1.63 Å in **Re/Si-M1**, showing the full formation of the B1−O2 bond in intermediates **Re/Si-M1** (Figure 2). The energy barrier (Figure 1) via transition state **Si-TS1** (0.96 kcal/mol) is calculated to be lower than that via transition state **Re-TS1** (1.79 kcal/mol); this should be the result of the larger steric hindrance between the oxazaborolidine ring and the phenyl ring in transition state **Re-TS1** than that in **Si-TS1**.

3.1.2. ***Second Step:*** *The C−C Bond Formation.* As shown in Figure 3A, the carbonyl group is situated above the phenyl group in the newly formed **Si-M1**, which effectively shields the Re-face (back) attack by the diazoester (**R2**). Thus, the nucleophilic addition of **R2** for construction of the C−C bond from the Si-face (front) of **Si-M1** should be facilitated.

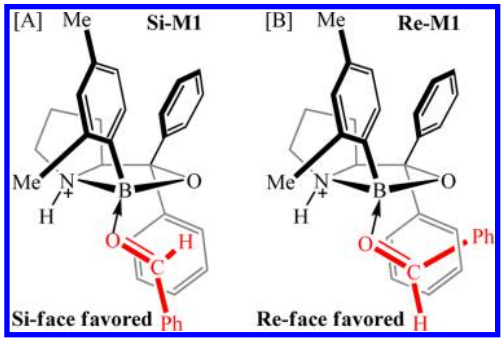

Figure 3. (A) Si-face coordination mode. (B) Re-face coordination mode.

Correspondingly, the nucleophilic addition of **R2** to **Re-M1** from the Re-face is favored (Figure 3B). Thus, there are four possible stereoselective reaction patterns (Scheme 3) for the nucleophilic attack on **Re/Si-M1** by the Re/Si-face of **R2** in the second step.

Scheme 3. Illustration of the Stereochemistry in the C−C Bond Formation Step

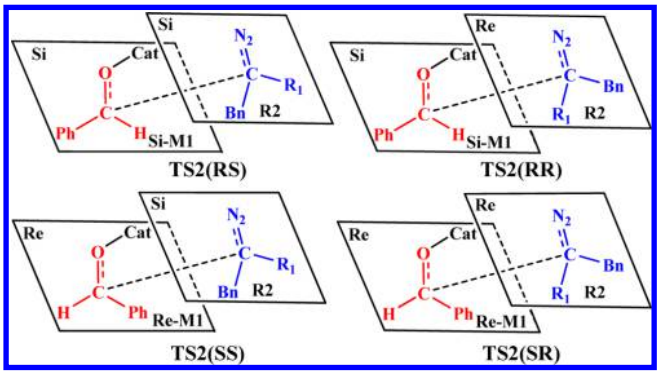

Those different nucleophilic attacks by the prochiral faces of **R2** create the two chiral carbon centers (i.e., C3 and C6 atoms) in the zwitterionic intermediate **M2(RR/RS/SR/SS)** via transition state **TS2(RR/RS/SR/SS)**. The appropriate alignments in this step are a prerequisite for the subsequent C−C/H insertion reaction.

As shown in Figure 4, the distances between C3 and C6 atoms are 1.96, 1.94, 2.02, and 2.06 Å in transition states **TS2(RR/RS/SR/SS)**, and are shortened to 1.64, 1.67, 1.61, and 1.60 Å in intermediates **M2(RR/RS/SR/SS)** (Figure S1 of the Supporting Information), which indicates that the C3−C6 bond is formed in this process. The energy barriers of the nucleophilic reaction via **TS2(RR/RS/SR/SS)** shown in Figure

DOI: 10.1021/acs.jpca.5b04793
J. Phys. Chem. A 2015, 119, 8422−8431

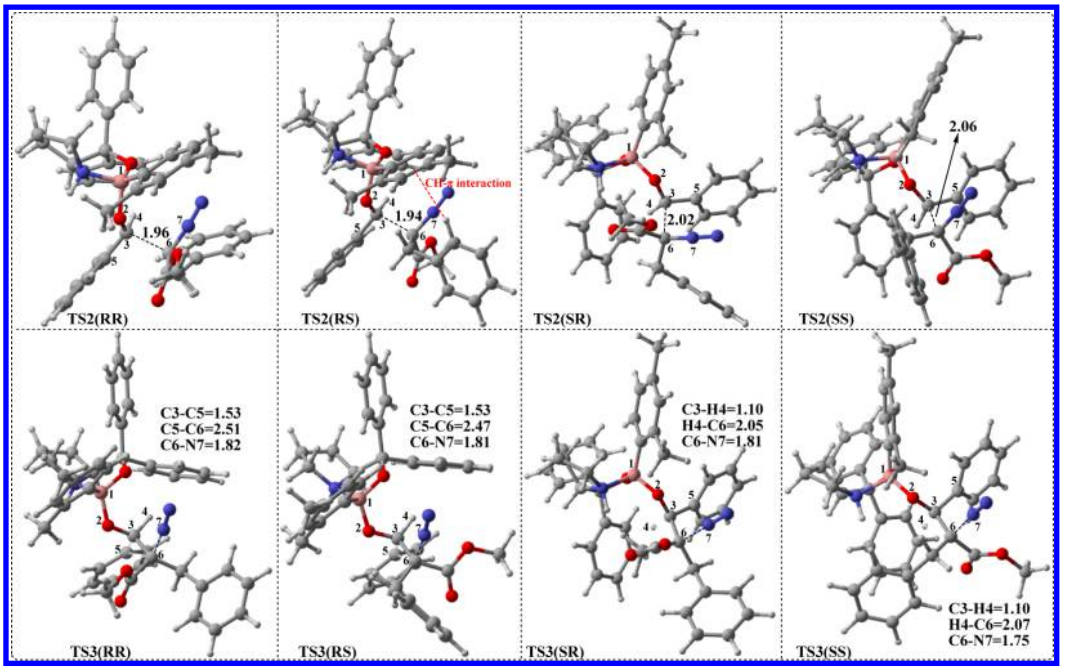

Figure 4. Key transition structures and geometrical parameters involved in the C−C/H insertion steps (distances in Å).

1 are 18.34, 13.53, 18.76, and 15.35 kcal/mol, respectively. The calculated results indicate that the formation of **M2**(**RS**/**SS**) is energetically favorable as compared to that of **M2**(**RR**/**SR**). The high energy barrier of transition state (**TS2RR**/**SR**) is generally explained in terms of the repulsion between the benzyl group of **R2** and the phenyl group of the N-protonated oxazaborolidine.

3.1.3. ***Third Step:*** *The Loss of Nitrogen Coupled with the Selective Migration of H/Ph.* As for the [1, 2]-H migration process shown in Scheme 2, the intermediate **M2**(**SR**/**SS**) transforms to the intermediate **H_M3**(***S***/***R***) via transition state **TS3**(**SR**/**SS**), while for the [1, 2]-Ph migration process, the intermediate **Ph_M3**(***R***/***S***) is obtained via transition state **TS3**(**RS**/**RR**). When the hydrogen locates on the same side with N_2 in **M2**(**SR**/**SS**), the N_2 shields the migration of the hydrogen; thus, the reaction will chemoselectively migrate the phenyl group for construction of the quaternary aldehyde. On the contrary, the N_2 will also prevent the migration of the phenyl group in **M2**(**RS**/**RR**), in which the phenyl group situates on the same side with N_2; thus, only the migration of hydrogen occurs. This interesting phenomenon should be resulting from the different alignment between **R2** and **Re**/**Si-M1** as discussed in the second step. It should be noted that the chirality of C3 atom in bold **R**/**S** disappears, and the chirality of C6 atom in bold and italic ***R***/***S*** changes to ***S***/***R*** correspondingly after the migration process.

The computational results reveal that the releasing of the nitrogen and the selective [1, 2]-H/Ph migration occur via a concerted but highly asynchronous transition state. Intrinsic reaction coordinate (IRC) calculations of the representative geometry **TS3**(**RS**) were performed to validate this concerted manner. The IRC results depicted in Figure 5 are associated with the structural transformation from transition state **TS3**(**RS**) to product **Ph_M3**(***R***). The formation of the C5−C6 bond proceeds throughout the course of the reaction, with instantaneous release of nitrogen (i.e., the breaking of bond C6−N7). For the Ph-migration transition state, the distance of C5−C6 was shortened from 2.51/2.47 Å in **TS3**(**RR**/**RS**) to

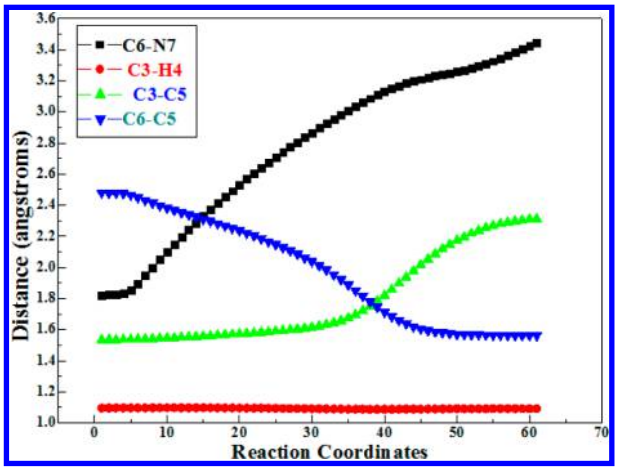

Figure 5. Changes in the key distances along IRC of **TS3**(**RS**).

1.55/1.55 Å in **Ph_M3**(***S***/***R***) (Supporting Information Figure S1). However, for these H-migration transition states, the distances H4−C6 are changed from 2.05/2.07 Å in **TS3**(**SR**/**SS**) to 1.09/1.10 Å in **H_M3**(***S***/***R***) (Supporting Information Figure S1). The energy barriers involved in those four pathways via transition states **TS3**(**RR**/**RS**/**SR**/**SS**) are 2.06, 2.36, 5.08, and 7.04 kcal/mol, respectively (Figure 1), indicating that the Ph/H-migration step is a facile process under the experimental conditions and the migration of phenyl group is preferential to the migration of hydrogen.

3.1.4. ***Fourth Step:*** *The Regeneration of Catalyst* ***Cat.*** In this step, the intermediate **Ph**/**H_M4**(***R***/***S***) is formed by the dissociation of the **Cat** via transition state **Ph**/**H_TS4**(***R***/***S***). The distances between B1 and O2 atoms are increased from 1.69, 1.69, 1.60, and 1.62 Å in intermediates **Ph_M3**(***S***), **Ph_M3**(***R***), **H_M3**(***S***), and **H_M3**(***R***) to 2.12, 2.11, 2.09, and 2.07 Å in transition states **Ph_TS4**(***S***), **Ph_TS4**(***R***), **H_TS4**(***S***), and **H_TS4**(***R***), respectively, revealing the break of the B1−O2 bond (Supporting Information Figure S1). The dissociation process via **Ph_TS4**(***S***), **Ph_TS4**(***R***), **H_TS4**(***S***),

DOI: 10.1021/acs.jpca.5b04793
J. Phys. Chem. A 2015, 119, 8422−8431

and **H_TS4(*R*)** costs 0.48, 0.58, 2.91, and 1.27 kcal/mol in relative energy with respect to the intermediates **Ph_M3(*S*)**, **Ph_M3(*R*)**, **H_M3(*S*)**, and **H_M3(*R*)**, respectively (Figure 1), which demonstrates that this step can occur smoothly; hence, it should be easy to regenerate the catalyst. Notably, these intermediates are formed by the weak interactions between the products and catalyst. Thus, the final products **Ph/H_P(*R*/*S*)** depicted in Scheme 1 should be obtained easily by the separation of the product with catalyst **Cat**.

3.2. Comparison of Oxazaborolidine with N-Protonated Oxazaborolidine. In order to compare the reactivity of N-protonated oxazaborolidine with that of oxazaborolidine, we have tried but failed to locate the coordinating transition structure of oxazaborolidine with aldehyde **R1**, and then we scanned the changes of key distance between them (Figure 6).

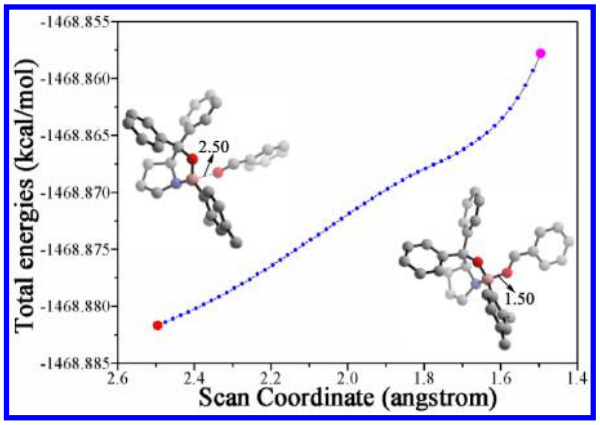

Figure 6. Scanning of distance B1−O2 between oxazaborolidine and aldehyde. The structures with the distance changing from 1.50 to 2.50 Å were optimized, and each distance change is 0.02 Å.

Figure 6 depicts that the energy of this complexation keeps increasing with aldehyde **R1** getting close to the oxazaborolidine. The coordination energy is estimated to be not lower than 15.69 kcal/mol, which should be much higher than the coordinate energy barrier for **R1** and the N-protonated oxazaborolidine via **Re/Si-TS1**, so we believe that the oxazaborolidine should be improper as the catalyst for this reaction.

Moreover, the frontier molecular orbital (FMO) analysis reveals that the energy gap between $HOMO_{R1}$ and $LUMO_{Cat}$ is 5.28 eV, while that between $HOMO_{R1}$ and the LUMO of oxazaborolidine is 6.25 eV (Figure 7). Obviously, the reaction between **R1** and oxazaborolidine cannot occur, which is because the energy gap is larger than 6 eV. It should be mentioned that the picture of $LUMO_{Cat}$ is very similar to that of oxazaborolidine, but the energy of $LUMO_{Cat}$ is lower by 0.93 eV than that of oxazaborolidine, indicating that the electron-accepting ability of the B1 atom in **Cat** is considerably stronger than that of oxazaborolidine. This signifies that the Lewis acidic character of the boron center is enhanced by the attachment of a proton to oxazaborolidine. In addition, the NBO analysis shows that the positive charges assigned on the B1 atom of oxazaborolidine and protonated oxazaborolidine are 1.061 and 1.157 e, respectively (Supporting Information Figure S2), demonstrating the electrophilicity of B1 atom in **Cat** is enhanced.

3.3. Origin of the Regio- and Stereoselectivity. For the organocatalytic reaction, it is important to figure out the factors

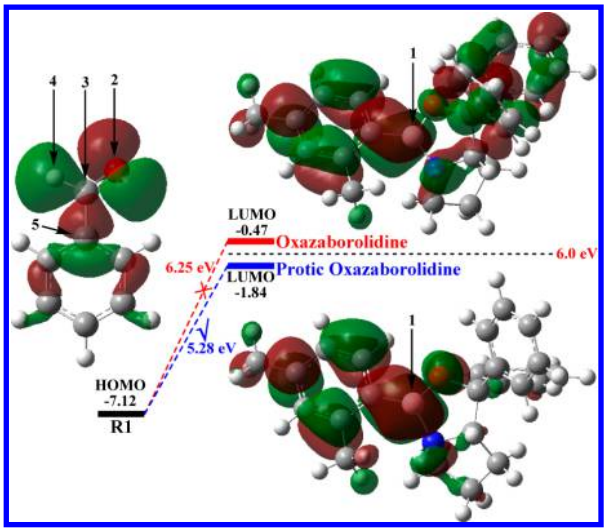

Figure 7. HOMO of aldehyde (**R1**), LUMO of oxazaborolidine, and LUMO of the protonated oxazaborolidine (**Cat**) calculated at B3LYP/6-31G(d, p) level in the propiontrile solvent.

governing the stereoselectivities[85,86] within the established mechanism. In order to explain the stereochemistry for the protonated oxazaborolidine-catalyzed asymmetric formal C−C insertion reaction, Ryu and co-workers proposed the possible transition state model (TS_{model}),[41] which was shown in Figure 8A. In their transition model, the phenyl group of the catalyst

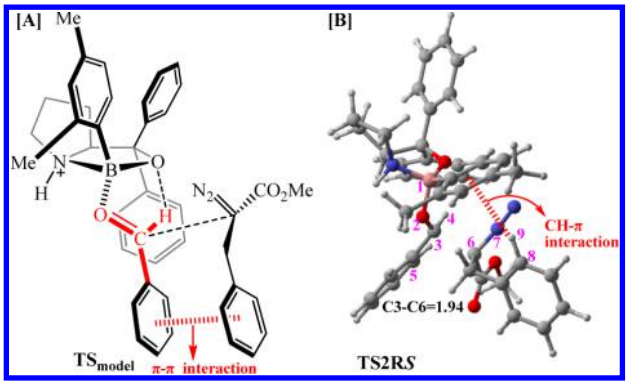

Figure 8. (A) Ryu's transition model (TS_{model}), (B) transition structures (**TS2(RS)**) optimized at the B3LYP/6-31G(d, p) level (distance is given in Å).

shields the Re-face (back) of **Si-M1** from attack by **R2**. Furthermore, the $\pi-\pi$ interaction between the benzyl group and phenyl group makes the nucleophilic attack of **R2** facilitated, and then gives the intermediate **Ph_M3(*R*)**. Actually, the $\pi-\pi$ interaction can hold the two aryl group together, but the benzyl group also shields the phenyl group migration in the third step. The following discussions should offer a reasonable explanation to the experimental fact that the formal C−C insertion reaction occurs more preferentially than the formal C−H insertion reaction, and the *R*-configuration is the major enantiomer.

As shown in Figure 1, the C−C bond formation step is calculated to be the stereoselectivity determining step. The four possible transition states **TS2(RR)**, **TS2(RS)**, **TS2(SR)**, and **TS2(SS)** are associated with the four stereoselective products **Ph_P(*S*)**, **Ph_P(*R*)**, **H_P(*S*)**, and **H_P(*R*)**, respectively. The energy barriers via **TS2(RR/RS/SR/SS)** shown in Figure 1 are

DOI: 10.1021/acs.jpca.5b04793
J. Phys. Chem. A 2015, 119, 8422−8431

18.34, 13.53, 18.76, and 15.35 kcal/mol, respectively. It is noteworthy that the lowest energy barrier for the migration of hydrogen (via **TS2(SS)**, 15.35 kcal/mol) is a little higher than that for the migration of the phenyl group (via **TS2(RS)**, 13.53 kcal/mol), so the α-benzyl-β-ketoester **H_P(*R*/*S*)** can still be obtained via the [1, 2]-hydrogen migration. The energy barrier of the favorable C−C insertion reaction pathway is 1.82 kcal/mol lower than that of the favorable C−H insertion reaction pathway, indicating that the C−C insertion reaction should be more energy favorable and **Ph_P(*R*)** should be the main product; this is in agreement with the experimental observations.

From the structural point of view, the reaction pathway via **TS2(RS)** associated with the *R*-configured product **Ph_P(*R*)** is calculated to be the most energetically favorable pathway. In a comparison with the four structures of key transition states involved in the second step, the large steric hindrance between the benzyl group of **R2** and phenyl group of oxazaborolidine leads to the higher energy barrier in transition state **TS2(RR/SR)**. While the transition state with C8 of the R2 pointing toward the aromic group of the catalyst (**TS2RS**, Figure 8B) is lower in energy than others due to a CH-π interaction between CH of **R2** and the aromatic ring of the catalyst. Specifically, the inner hydrogen on **R2** is just 2.36 Å from H9 to the aromatic group, which is within the combined van der Waals distance of 2.90 Å. On the whole, the CH-π interaction (Figure 8B) and the less steric repulsion hold the transition structure **TS2(RS)** much more stable than the other transition structures. Thus, the *R*-configured aldehyde **Ph_P(*R*)** is the major enantiomer among the four stereoselective products. The computed energy difference between the two key transition states **TS2(RS/RR)** associated with the products **Ph_P(*R*/*S*)** is 4.81 kcal/mol, which corresponds to the enantiomeric excess of >99% in favor of the *R* isomer. This is in line with the experimentally observed ee of 97%.

3.4. Analysis of the Global Reactivity Indexes. In order to understand the role of the Lewis acid catalyst **Cat** in depth, we have performed an analysis of the global reactivity indexes (GRIs) of the reactants before and after the absorption by catalyst. The molecule global electrophilicity character is measured by electrophilicity index, ω, which has been given from the following expression, $\omega = (\mu^2/2\eta)$,[87−89] in terms of the electronic chemical potential μ and the chemical hardness η. Both quantities may be approached in terms of the one-electron energies of the frontier molecular orbital HOMO and LUMO, E_H and E_L, as $\mu \approx (E_H - E_L)/2$ and $\eta \approx (E_L - E_H)$. Moreover, according the HOMO energies obtained within the Kohn−Sham scheme,[90,91] Domingo and co-workers gave the nucleophilicity index N to handle a nucleophilicity scale.[92−94] The nucleophilicity index is defined as $N = E_{H(SR)} - E_{H(TCE)}$. This nucleophilicity scale is referred to tetracyanoethylene (TCE) taken as reference. Following these indices definition, in this reaction (Table 1), **R2** is classified as the nucleophile with the nucleophilicity index of 2.456 eV. **R1** and **Re/Si-M1** are electrophiles with the values of 1.870, 3.612, and 3.662 eV, respectively. Obviously, the coordination of catalyst **Cat** to aldehyde carbon atom of **R1** noticeably strengthens the electrophilicity of **R1**, and thus promotes the formal C−C/H insertion reaction. The GRI analysis further revealed that the oxazaborolidine cannot catalyze the insertion reaction due to the lower nucleophilicity of oxazaborolidine-aldehyde complex **M1$_{oxa}$**.

Table 1. Energies of HOMO (E_L, au) and LUMO (E_L, au), Electronic Chemical Potential (μ, au), Chemical Hardness (η, au), Global Electrophilicity (ω, eV), and Global Nucleophilicity (N, eV) of Some Reactants (SR)

SR	E_H (au)	E_L (au)	μ (au)	η (au)	ω (ev)	N^a (eV)
R1	−0.26164	−0.06616	−0.164	0.195	1.870	1.636
R2	−0.23151	−0.06616	−0.149	0.165	1.823	2.456
Si-M1	−0.23878	−0.11855	−0.179	0.120	3.612	2.258
Re-M1	−0.24103	−0.11997	−0.181	0.121	3.662	2.197
M1$_{oxa}$	−0.28339	0.02077	−0.152	0.304	0.038	0.038

[a] $E_{H(TCE)}$ = −0.32177 au (calculated at B3LYP/6-31G(d, p)/IEF-PCM (propionitrile).

4. CONCLUSIONS

In summary, the possible reaction mechanisms and stereoselectivities of the formal C−C/H insertion reaction between aldehyde and diazoaester catalyzed by N-protonated chiral oxazaborolidine have been studied theoretically. Four kinds of stereoselective reaction pathways are investigated and compared in detail. We have located the transition state, which is leading to the major or minor products in the experiment reported by Ryu and co-workers. The calculated results indicate that the pathway associated with the migration of phenyl group is more energetically favorable than the pathway associated with the migration of hydrogen, which is consistent with the regioselective results in the experiments.

The computational results reveal that the C−C bond formation step is the stereoselectivity determining step. Thus, the C−C bond formation step would be the key for the stereoselectivity of the reaction, and the CH-π interaction as well as the less steric repulsion in the favorable transition state **TS2(RS)** should be responsible for the stereoselectivity of the reaction.

It is noteworthy that our results found that it is hard for oxazaborolidine to coordinate with aldehyde directly, because the Lewis acidity of boron atom is largely reduced without attachment of a proton. Actually, the attachment of the proton strengthens the Lewis acidity of boron center in oxazaborolidine by polarizing the B−N bond to make the boron center more electron-deficient. The GRI analysis reveals that the coordination of the proton significantly enhances the electron-accepting ability of aldehyde, which is also identified by the IRC scanning results as well as the FMO analysis. This would provide a convenient way to predict the reactivity of this kind of catalyst. As described in concerns above, this theoretical study would be useful for understanding the detailed mechanism and selectivities of the insertion reactions, and also provides valuable insights on the rational designs of the Lewis acid catalysts for this kind of reaction.

■ ASSOCIATED CONTENT

Supporting Information

Cartesian coordinates, NBO charge distribution of oxazaborolidine and N-protonated oxazaborolidine, another proposed reaction mechanism, the optimized structures and geometrical parameters, the comparison of the key transition states calculated by the different methods, the energies of all the stationary points, and the complete citation of ref 65. The Supporting Information is available free of charge on the ACS Publications website at DOI: 10.1021/acs.jpca.5b04793.

DOI: 10.1021/acs.jpca.5b04793
J. Phys. Chem. A 2015, 119, 8422−8431

AUTHOR INFORMATION

Corresponding Authors

*E-mail: mstang@zzu.edu.cn.

*E-mail: donghuiwei@zzu.edu.cn. Phone: +86 037167781815.

Notes

The authors declare no competing financial interest.

ACKNOWLEDGMENTS

We acknowledge financial support from the National Natural Science Foundation of China (No. 21303167), China Postdoctoral Science Foundation (No. 2013M530340), and Excellent Doctoral Dissertation Engagement Fund of Zhengzhou University in 2014.

REFERENCES

(1) De Vries, T. S.; Prokofjevs, A.; Vedejs, E. Cationic Tricoordinate Boron Intermediates: Borenium Chemistry from the Organic Perspective. *Chem. Rev.* **2012**, *112*, 4246−4282.

(2) Dimitrijević, E.; Taylor, M. S. Organoboron Acids and Their Derivatives as Catalysts for Organic Synthesis. *ACS Catal.* **2013**, *3*, 945−962.

(3) Stahl, T.; Klare, H. F. T.; Oestreich, M. Main-Group Lewis Acids for C−F Bond Activation. *ACS Catal.* **2013**, *3*, 1578−1587.

(4) Balucani, N.; Zhang, F. T.; Kaiser, R. I. Elementary Reactions of Boron Atoms with Hydrocarbons-Toward the Formation of Organo-Boron Compounds. *Chem. Rev.* **2010**, *110*, 5107−5127.

(5) Candeias, N. R.; Montalbano, F.; Cal, P. M. S. D.; Gois, P. M. P. Boronic Acids and Esters in the Petasis-Borono Mannich Multi-component Reaction. *Chem. Rev.* **2010**, *110*, 6169−6193.

(6) Deloux, L.; Srebnik, M. Asymmetric Boron-Catalyzed Reactions. *Chem. Rev.* **1993**, *93*, 763−784.

(7) Burkhardt, E. R.; Matos, K. Boron Reagents in Process Chemsitry: Excellent Tools for Selective Reductions. *Chem. Rev.* **2006**, *106*, 2617−2650.

(8) Piers, W. E.; Bourke, S. C.; Conroy, K. D. Borinium, Borenium, and Boronium Ions: Synthesis, Reactivity, and Applications. *Angew. Chem., Int. Ed.* **2005**, *44*, 5016−5036.

(9) Yamamoto, H.; Futatsugi, K. "Designer Acids": Combined Acid Catalysis for Asymmetric Synthesis. *Angew. Chem., Int. Ed.* **2005**, *44*, 1924−1942.

(10) Corey, E. J.; Bakshi, R. K.; Shibata, S. Highly Enantioselective Borane Reduction of Ketones Catalyzed by Chiral Oxazaborolidines. Mechanism and Synthetic Implications. *J. Am. Chem. Soc.* **1987**, *109*, 5551−5553.

(11) Corey, E. J.; Bakshi, R. K.; Shibata, S.; Chen, C. P.; Singh, V. K. A Stable and Easily Prepared Catalyst for the Enantioselective Reduction of Ketones. Applications to Multistep Syntheses. *J. Am. Chem. Soc.* **1987**, *109*, 7925−7926.

(12) Demir, A. S.; Sesenoglu, O.; Gercek-Arkin, Z. An Asymmetric Synthesis of Both Enantiomers of 2,2,2-Trifluoro-1-furan-2-yl-ethylamine and 3,3,3-Trifluoroalanine from 2,2,2-Trifluoro-1-furan-2-yl-ethanone. *Tetrahedron: Asymmetry* **2001**, *12*, 2309−2313.

(13) Demir, A. S.; Sesenoglu, O.; Aksoy-Cam, H.; Kaya, H.; Aydogan, K. Enantioselective Synthesis of Both Enantiomers of 2-Amino-2-(2-furyl)ethan-1-ol as a Flexible Building Block for the Preparation of Serine and Azasugars. *Tetrahedron: Asymmetry* **2003**, *14*, 1335−1340.

(14) Kirton, E. H. M.; Tughan, G.; Morris, R. E.; Field, R. A. Rationalising the Effect of Reducing Agent on the Oxazaborolidine-mediated Asymmetric Reduction of N-substituted Imines. *Tetrahedron Lett.* **2004**, *45*, 853−855.

(15) Gosselin, F.; O'Shea, P. D.; Roy, S.; Reamer, R. A.; Chen, C. Y.; Volante, R. P. Unprecedented catalytic asymmetric reduction of N-H imines. *Org. Lett.* **2005**, *7*, 355−358.

(16) Ryu, D. H.; Lee, T. W.; Corey, E. J. Broad-Spectrum Enantioselective Diels-Alder Catalysis by Chiral, Cationic Oxazaborolidines. *J. Am. Chem. Soc.* **2002**, *124*, 9992−9993.

(17) Ryu, D. H.; Corey, E. J. Triflimide Activation of a Chiral Oxazaborolidine Leads to a More General Catalytic System for Enantioselective Diels-Alder Addition. *J. Am. Chem. Soc.* **2003**, *125*, 6388−6390.

(18) Ryu, D. H.; Zhou, G.; Corey, E. J. Enantioselective and Structure-Selective Diels-Alder Reactions of Unsymmetrical Quinones Catalyzed by a Chiral Oxazaborolidinium Cation. Predictive Selection Rules. *J. Am. Chem. Soc.* **2004**, *126*, 4800−4802.

(19) Canales, E.; Corey, E. J. Highly Enantioselective [4 + 2] Cycloaddition Reactions Catalyzed by a Chiral N-Methyl-oxazaborolidinium Cation. *Org. Lett.* **2008**, *10*, 3271−3273.

(20) Payette, J. N.; Yamamoto, H. Regioselective and Asymmetric Diels-Alder Reaction of 1- and 2-Substituted Cyclopentadienes Catalyzed by a Brønsted Acid Activated Chiral Oxazaborolidine. *J. Am. Chem. Soc.* **2007**, *129*, 9536−9537.

(21) Shibatomi, K.; Futatsugi, K.; Kobayashi, F.; Iwasa, S.; Yamamoto, H. Stereoselective Construction of Halogenated Quaternary Stereogenic Centers via Catalytic Asymmetric Diels-Alder Reaction. *J. Am. Chem. Soc.* **2010**, *132*, 5625−5627.

(22) Paddon-Row, M. N.; Kwan, L. C. H.; Willis, A. C.; Sherburn, M. S. Enantioselective Oxazaborolidinium-Catalyzed Diels-Alder Reactions without CH···O Hydrogen Bonding. *Angew. Chem., Int. Ed.* **2008**, *47*, 7013−7017.

(23) Sakata, K.; Fujimoto, H. Quantum Chemical Study of Diels-Alder Reactions Catalyzed by Lewis Acid Activated Oxazaborolidines. *J. Org. Chem.* **2013**, *78*, 3095−3103.

(24) Omar, N. Y. M.; Rahman, N. A.; Zain, S. M. Enantioselective Organocatalytic Diels-Alder Reactions: A Density Functional Theory and Kinetic Isotope Effects Study. *J. Comput. Chem.* **2011**, *32*, 1813−1823.

(25) Paddon-Row, M. N.; Anderson, C. D.; Houk, K. N. Computational Evaluation of Enantioselective Diels-Alder Reactions Mediated by Corey's Cationic Oxazaborolidine Catalysts. *J. Org. Chem.* **2009**, *74*, 861−868.

(26) Canales, E.; Corey, E. J. Highly Enantioselective [2 + 2]-Cycloaddition Reactions Catalyzed by a Chiral Aluminum Bromide Complex. *J. Am. Chem. Soc.* **2007**, *129*, 12686−12687.

(27) Zhou, G.; Corey, E. J. Short, Enantioselective Total Synthesis of Aflatoxin B-2 Using An Asymmetric [3 + 2]-Cycloaddition Step. *J. Am. Chem. Soc.* **2005**, *127*, 11958−11959.

(28) Gao, L.; Hwang, G. S.; Lee, M. Y.; Ryu, D. H. Catalytic Enantioselective 1,3-Dipolar Cycloadditions of Alkyl Diazoacetates with alpha,beta-Disubstituted Acroleins. *Chem. Commun.* **2009**, 5460−5462.

(29) Zhou, G.; Hu, Q. Y.; Corey, E. J. Useful Enantioselective Bicyclization Reactions Using an N-protonated Chiral Oxazaborolidine As Catalyst. *Org. Lett.* **2003**, *5*, 3979−3982.

(30) Ryu, D. H.; Corey, E. J. Highly Enantioselective Cyanosilylation of Aldehydes Catalyzed by a Chiral Oxazaborolidinium Ion. *J. Am. Chem. Soc.* **2004**, *126*, 8106−8107.

(31) Ryu, D. H.; Corey, E. J. Enantioselective Cyanosilylation of Ketones Catalyzed by a Chiral Oxazaborolidinium ion. *J. Am. Chem. Soc.* **2005**, *127*, 5384−5387.

(32) Liu, D.; Hong, S. W.; Corey, E. J. Enantioselective Synthesis of Bridged- or Fused-ring Bicyclic Ketones by a Catalytic Asymmetric Michael Addition Pathway. *J. Am. Chem. Soc.* **2006**, *128*, 8160−8161.

(33) Ishihara, K.; Kondo, S.; Yamamoto, H. Scope and Limitations of Chiral B-[3,5-Bis(trifluoromethyl)phenyl]oxazaborolidine Catalyst for Use in the Mukaiyama Aldol Reaction. *J. Org. Chem.* **2000**, *65*, 9125−9128.

(34) Senapati, B. K.; Gao, L.; Lee, S. I.; Hwang, G. S.; Ryu, D. H. Highly Enantioselective Mukaiyama Aldol Reactions Catalyzed by a Chiral Oxazaborolidinium Ion: Total Synthesis of (−)-Inthomycin C. *Org. Lett.* **2010**, *12*, 5088−5091.

(35) Larionov, O. V.; Corey, E. J. An Unconventional Approach to the Enantioselective Synthesis of Caryophylloids. *J. Am. Chem. Soc.* **2008**, *130*, 2954−2955.

(36) VanHeyst, M. D.; Oblak, E. Z.; Wright, D. L. Stereodivergent Resolution of Oxabicyclic Ketones: Preparation of Key Intermediates

DOI: 10.1021/acs.jpca.5b04793
J. Phys. Chem. A 2015, 119, 8422−8431

for Platensimycin and Other Natural Products. *J. Org. Chem.* **2013**, *78*, 10555−10559.
(37) Ovaska, T. V.; Sullivan, J. A.; Ovaska, S. I.; Winegrad, J. B.; Fair, J. D. Asymmetric Synthesis of Seven-Membered Carbocyclic Rings via a Sequential Oxyanionic 5-Exo-Dig Cyclization/Claisen Rearrangement Process. Total Synthesis of (−)-Frondosin B. *Org. Lett.* **2009**, *11*, 2715−2718.
(38) Lee, S. I.; Hwang, G. S.; Ryu, D. H. Catalytic Enantioselective Carbon Insertion into the beta-Vinyl C-H Bond of Cyclic Enones. *J. Am. Chem. Soc.* **2013**, *135*, 7126−7129.
(39) Gao, L. Z.; Kang, B. C.; Hwang, G. S.; Ryu, D. H. Enantioselective Synthesis of alpha-Alkyl-beta-ketoesters: Asymmetric Roskamp Reaction Catalyzed by an Oxazaborolidinium Ion. *Angew. Chem., Int. Ed.* **2012**, *51*, 8322−8325.
(40) Lee, S. I.; Kang, B. C.; Hwang, G. S.; Ryu, D. H. Catalytic Carbon Insertion into the beta-Vinyl C-H Bond of Cyclic Enones with Alkyl Diazoacetates. *Org. Lett.* **2013**, *15*, 1428−1431.
(41) Gao, L.; Kang, B. C.; Ryu, D. H. Catalytic Asymmetric Insertion of Diazoesters into Aryl-CHO Bonds: Highly Enantioselective Construction of Chiral All-Carbon Quaternary Centers. *J. Am. Chem. Soc.* **2013**, *135*, 14556−14559.
(42) Qiao, Y.; Han, K. L. Elucidation of the Reaction Mechanisms and Diastereoselectivities of Phosphine-catalyzed [4 + 2] Annulations between Allenoates and Ketones or Aldimines. *Org. Biomol. Chem.* **2012**, *10*, 7689−7706.
(43) Qiao, Y.; Han, K. L. Theoretical Investigations Toward the Tandem Reactions of N-aziridinyl Imine Compounds Forming Triquinanes via Trimethylenemethane Diyls: Mechanisms and Stereoselectivity. *Org. Biomol. Chem.* **2014**, *12*, 1220−1231.
(44) Wang, Y.; Wei, D. H.; Zhang, W. J.; Wang, Y. Y.; Zhu, Y. Y.; Jia, Y.; Tang, M. S. A Theoretical Study on the Mechanisms of the Reactions between 1,3-Dialkynes and Ammonia Derivatives for the Formation of Five-membered N-heterocycles. *Org. Biomol. Chem.* **2014**, *12*, 7503−7514.
(45) Zhang, L.; Fang, D. C. Catalytic C-H Activation/C-C Coupling Reaction: DFT Studies on theMechanism, Solvent Effect, and Role of Additive. *J. Org. Chem.* **2013**, *78*, 2405−2412.
(46) Xing, Y. M.; Zhang, L.; Fang, D. C. DFT Studies on the Mechanism of Palladium(IV)-Mediated C-H Activation Reactions: Oxidant Effect and Regioselectivity. *Organometallics* **2015**, *34*, 770−777.
(47) Tao, J. Y.; Fang, D. C.; Chass, G. A. Simplification Through Complexity: the Role of Ni-complexes in Catalysed Diyne-cyclobutanone [4 + 2+2] Cycloadditions, A Comparative DFT Study. *Phys. Chem. Chem. Phys.* **2012**, *14*, 6937−6945.
(48) Louie, M. K.; Francisco, J. S.; Verdicchio, M.; Klippenstein, S. J.; Sinha, A. Hydrolysis of Ketene Catalyzed by Formic Acid: Modification of Reaction Mechanism, Energetics, and Kinetics with Organic Acid Catalysis. *J. Phys. Chem. A* **2015**, *119*, 4347−4357.
(49) Rypkema, H. A.; Sinha, A.; Francisco, J. S. Carboxylic Acid Catalyzed Hydration of Acetaldehyde. *J. Phys. Chem. A* **2015**, *119*, 4581−4588.
(50) Wang, Y.; Zheng, L. J.; Wei, D. H.; Tang, M. S. Quantum Mechanical Study of Mechanism and Stereoselectivity on the N-heterocyclic Carbene Catalyzed [4 + 2] Annulation Reaction of Enals with Azodicarboxylates. *Org. Chem. Front.* **2015**, DOI: 10.1039/C5QO00121H.
(51) Qiao, Y.; Han, K. L.; Zhan, C. G. Fundamental Reaction Pathway and Free Energy Profile for Butyrylcholinesterase-Catalyzed Hydrolysis of Heroin. *Biochemistry* **2013**, *52*, 6467−6479.
(52) Qiao, Y.; Han, K. L.; Zhan, C. G. Reaction Pathways and free Energy Profiles for Cholinesterase-catalyzed Hydrolysis of 6-Monoacetylmorphine. *Org. Biomol. Chem.* **2014**, *12*, 2214−2227.
(53) Li, D. M.; Wang, Y.; Han, K. L. Recent Density Functional Theory Model Calculations of Drug Metabolism by Cytochrome P450. *Coord. Chem. Rev.* **2012**, *256*, 1137−1150.
(54) Wei, D. H.; Tang, M. S.; Zhan, C. G. Fundamental Reaction Pathway and Free Energy Profile for Proteasome Inhibition by Syringolin A (SylA). *Org. Biomol. Chem.* **2015**, *13*, 6857−6865.
(55) Wei, D. H.; Lei, B. L.; Tang, M. S.; Zhan, C. G. Fundamental Reaction Pathway and Free Energy Profile for Inhibition of Proteasome by Epoxomicin. *J. Am. Chem. Soc.* **2012**, *134*, 10436−10450.
(56) Li, Y.; Fang, D. C. DFT Calculations on Kinetic Data for Some [4 + 2] Reactions in Solution. *Phys. Chem. Chem. Phys.* **2014**, *16*, 15224−15230.
(57) Chen, Y. M.; Chass, G. A.; Fang, D. C. Between A Reactant Rock and A Solvent Hard Place -molecular Corrals Guide Aromatic Substitutions. *Phys. Chem. Chem. Phys.* **2014**, *16*, 1078−1083.
(58) Le, X. T.; Mai, T. V. T.; Ratkiewicz, A.; Huynh, L. K. Mechanism and Kinetics of Low-Temperature Oxidation of a Biodiesel Surrogate: Methyl Propanoate Radicals with Oxygen Molecule. *J. Phys. Chem. A* **2015**, *119*, 3689−3703.
(59) Zheng, J.; Zhuang, X. H.; Qiu, L.; Xie, Y.; Wan, X. B.; Lan, Z. G. Antiaromatic Characteristic Analysis of 1,4-Diazapentalene Derivatives: A Theoretical Study. *J. Phys. Chem. A* **2015**, *119*, 3762−3769.
(60) Lv, S. S.; Liu, Y. R.; Huang, T.; Feng, Y. J.; Jiang, S.; Huang, W. Stability of Hydrated Methylamine: Structural Characteristics and $H_2N\cdots$H-O Hydrogen Bonds. *J. Phys. Chem. A* **2015**, *119*, 3770−3779.
(61) Rosokha, S. V.; Loboda, E. A. Interplay of Halogen and $\pi-\pi$ Charge-Transfer Bondings in Intermolecular Associates of Bromo- or Iododinitrobenzene with Tetramethyl-p-phenylenediamine. *J. Phys. Chem. A* **2015**, *119*, 3833−3842.
(62) Becke, A. D. Density-Functional Thermochemistry 0.3. The Role of Exact Exchange. *J. Chem. Phys.* **1993**, *98*, 5648−5652.
(63) Lee, C. T.; Yang, W. T.; Parr, R. G. Development of the Colle-Salvetti Correlation-Energy Formula into a Functional of the Electron-Density. *Phys. Rev. B: Condens. Matter Mater. Phys.* **1988**, *37*, 785−789.
(64) Miehlich, B.; Savin, A.; Stoll, H.; Preuss, H. Results Obtained with the Correlation-Energy Density Functionals of Becke and Lee, Yang and Parr. *Chem. Phys. Lett.* **1989**, *157*, 200−206.
(65) Frisch, M. J.; Trucks, G. W.; Schlegel, H. B.; Scuseria, G. E.; Robb, M. A.; Cheeseman, J. R.; Scalmani, G.; Barone, V.; Mennucci, B.; Petersson, G. A.; et al. *Gaussian 09, Revision C.01*; Gaussian, Inc.: Wallingford, CT, 2010.
(66) Sun, L.; Tang, M. S.; Wang, M. H.; Wei, D. H.; Liu, L. L. A Theoretical Investigation of the Enantioselective Reduction of Prochiral Ketones Promoted by Chiral Diamines. *Tetrahedron: Asymmetry* **2008**, *19*, 779−787.
(67) Alagona, G.; Ghio, C.; Tomasi, S. Theoretical Investigation on the Oxazaborolidine-ketone Interaction in Small Model Systems. *Theor. Chem. Acc.* **2004**, *111*, 287−302.
(68) Cheong, P. H. Y.; Legault, C. Y.; Um, J. M.; Celebi-Olcum, N.; Houk, K. N. Quantum Mechanical Investigations of Organocatalysis: Mechanisms, Reactivities, and Selectivities. *Chem. Rev.* **2011**, *111*, 5042−5137.
(69) Wei, D. H.; Tang, M. S.; Zhang, W. J.; Zhao, J.; Sun, L.; Zhao, C. F.; Wang, H. M. A Density Functional Theory Study of the Enantioselective Reduction of Prochiral Ketones Promoted by Chiral Spiroborate Esters. *Int. J. Quantum Chem.* **2011**, *111*, 596−605.
(70) Wei, D. H.; Tang, M. S.; Zhao, J.; Sun, L.; Zhang, W. J.; Zhao, C. F.; Zhang, S. R.; Wang, H. M. A DFT Study of the Enantioselective Reduction of Prochiral Ketones Promoted by Pinene-derived Amino Alcohols. *Tetrahedron: Asymmetry* **2009**, *20*, 1020−1026.
(71) Wang, Y.; Wei, D. H.; Li, Z. Y.; Zhu, Y. Y.; Tang, M. S. DFT Study on the Mechanisms and Diastereoselectivities of Lewis Acid-Promoted Ketene-Alkene [2 + 2] Cycloadditions: What is the Role of Lewis Acid in the Ketene and C = X (X = O, CH2, and NH) [2 + 2] Cycloaddition Reactions? *J. Phys. Chem. A* **2014**, *118*, 4288−4300.
(72) Wei, D. H.; Zhang, W. J.; Zhu, Y. Y.; Tang, M. S. A DFT Study on the Reaction Mechanisms of Ketene-ketone [2 + 2+2] Cycloaddition to Form 3-Aryglutaric Anhydrides Under a Lewis Acid Catalysis: What is the Role of BF_3? *J. Mol. Catal. A: Chem.* **2010**, *326*, 41−47.
(73) Li, Q. G.; Xu, K.; Yi, R. Origin of Enhanced Reactivity of a Microsolvated Nucleophile in Ion Pair SN2 Reactions: The Cases of Sodium p-Nitrophenoxide with Halomethanes in Acetone. *J. Phys. Chem. A* **2015**, *119*, 3878−3886.

DOI: 10.1021/acs.jpca.5b04793
J. Phys. Chem. A 2015, 119, 8422−8431

(74) Sharipov, A. S.; Starik, A. M. Theoretical Study of the Reactions of Ethanol with Aluminum and Aluminum Oxide. *J. Phys. Chem. A* **2015**, *119*, 3897−3904.
(75) Wang, Y. Y.; Wang, Y.; Zhang, W. J.; Zhu, Y. Y.; Wei, D. H.; Tang, M. S. Mechanisms and Stereoselectivities of Rh(I)-catalyzed Carbenoid Carbon Insertion Reaction of Benzocyclobutenol with Diazoester. *Org. Biomol. Chem.* **2015**, *13*, 6587−6597.
(76) Barone, V.; Cossi, M. Quantum Calculation of Molecular Energies and Energy Gradients in Solution by a Conductor Solvent Model. *J. Phys. Chem. A* **1998**, *102*, 1995−2001.
(77) Mennucci, B.; Tomasi, J. Continuum Solvation Models: A New Approach to the Problem of Solute's Charge Distribution and Cavity Boundaries. *J. Chem. Phys.* **1997**, *106*, 5151−5158.
(78) Legault, C. Y. *CYLView, 1.0b*; Université de Sherbrooke: Sherbrooke, Quebec, Canada, 2009; http://www.cylview.org.
(79) Gonzalez, C.; Schlegel, H. B. An Improved Algorithm for Reaction-Path Following. *J. Chem. Phys.* **1989**, *90*, 2154−2161.
(80) Gonzalez, C.; Schlegel, H. B. Reaction-Path Following in Mass-Weighted Internal Coordinates. *J. Phys. Chem.* **1990**, *94*, 5523−5527.
(81) Reed, A. E.; Weinhold, F. J. Natural Bond Orbital Analysis of Near-Hartree-Fock Water Dimmer. *J. Chem. Phys.* **1983**, *78*, 4066−4073.
(82) Foster, J. P.; Weinhold, F. J. Natural Hybrid Orbitals. *J. Am. Chem. Soc.* **1980**, *102*, 7211−7218.
(83) Glendening, E. D.; Reed, A. E.; Carpenter, J. E.; Weinhold, F. J. *NBO Version 3.1*.
(84) Chen, X. F.; Zhang, X.; Han, K. L.; Varandas, A. J. C. Ab Initio Study of the H + $ClONO_2$ Reaction. *Chem. Phys. Lett.* **2006**, *421*, 453−459.
(85) Chen, X. F.; Hou, C. Y.; Han, K. L. DFT Study of Intermolecular [4 + 2] versus [3 + 2] Cycloadditions in the Dimerization of 2,4,6-Trinitrotoluene (TNT): Regioselectivity and Stereoselectivity. *J. Phys. Chem. A* **2010**, *114*, 1169−1177.
(86) Li, D. M.; Huang, X. Q.; Han, K. L.; Zhan, C. G. Catalytic Mechanism of Cytochrome P450 for 5′-Hydroxylation of Nicotine: Fundamental Reaction Pathways and Stereoselectivity. *J. Am. Chem. Soc.* **2011**, *133*, 7416−7427.
(87) Parr, R. G.; Pearson, R. G. Absolute Hardness-Companion Parameter to Absolute Electronegativity. *J. Am. Chem. Soc.* **1983**, *105*, 7512−7516.
(88) Domingo, L. R.; Picher, M. T.; Saez, J. A. Toward an Understanding of the Unexpected Regioselective Hetero-Diels-Alder Reactions of Asymmetric Tetrazines with Electron-Rich Ethylenes: A DFT Study. *J. Org. Chem.* **2009**, *74*, 2726−2735.
(89) Domingo, L. R.; Aurell, M. J.; Perez, P.; Contreras, R. Quantitative Characterization of the Global Electrophilicity Power of Common Diene/dienophile Pairs in Diels-Alder Reactions. *Tetrahedron* **2002**, *58*, 4417−4423.
(90) Sham, L. J.; Kohn, W. 1-Particle Properties of an Inhomogeneous Interacting Electron Gas. *Phys. Rev.* **1966**, *145*, 561−567.
(91) Kohn, W.; Sham, L. J. Quantum Density Oscillations in an Inhomogeneous Electron Gas. *Phys. Rev.* **1965**, *137*, 1697−1705.
(92) Domingo, L. R.; Perez, P.; Saez, J. A. Understanding the Local Reactivity in Polar Organic Reactions Through Electrophilic and Nucleophilic Parr Functions. *RSC Adv.* **2013**, *3*, 1486−1494.
(93) Domingo, L. R.; Chamorro, E.; Perez, P. An Analysis of the Regioselectivity of 1,3-Dipolar Cycloaddition Reactions of Benzonitrile N-Oxides Based on Global and Local Electrophilicity and Nucleophilicity Indices. *Eur. J. Org. Chem.* **2009**, *2009*, 3036−3044.
(94) Domingo, L. R.; Chamorro, E.; Perez, P. An Understanding of the Electrophilic/nucleophilic Behavior of Electro-deficient 2,3-Disubstituted 1,3-Butadienes in Polar Diels-Alder Reactions. A Density Functional Theory Study. *J. Phys. Chem. A* **2008**, *112*, 4046−4053.

DOI: 10.1021/acs.jpca.5b04793
J. Phys. Chem. A 2015, 119, 8422−8431